Hindawi
Geofluids
Volume 2022, Article ID 4563438, 15 pages
https://doi.org/10.1155/2022/4563438

Research Article

Effects of Injection Pressure and Duration on Alternate High-Pressure Water-Gas Sequestration of Coalbed Methane

Ke Li, Chuanjie Zhu, Siyuan Liu, Deliang Chen, and Guanghui Cai

Faculty of Safety Engineering, China University of Mining and Technology, Xuzhou, Jiangsu 221116, China

Correspondence should be addressed to Chuanjie Zhu; anq021@126.com

Received 17 September 2022; Revised 4 November 2022; Accepted 7 November 2022; Published 30 November 2022

Academic Editor: Zhiyuan Wang

To solve the problems of high ground stress, low permeability and low coalbed methane recovery, this paper proposes an optimization technique for improving coal seam permeability, i.e., water-gas alternating displacement enhances coalbed methane recovery (WGA-ECBM). The seepage field of gas-water two-phase flow is derived and a multiphase fluid-solid coupling model between physical parameters is established. This paper studies the effects of three displacement methods (water injection, air injection and water-air alternating injection) on methane recovery. The influence of injection pressure and injection duration on the WGA-ECBM technique is also studied. The V_{CH_4} (methane volume fraction) of the three methods decrease by 17.84%, 12.72% and 44.62% in the borehole, respectively. The influence ranges (diameter) are 24.68 m, 149.73 m and 135.21 m, respectively. Pore pressures and displacement area also increase as injection pressure increases in a 5 MPa gradient. And V_{CH_4} in the borehole decrease by 35.57%, 43.82%, 46.78% and 51.72% from 10 MPa to 25 MPa, respectively. With the increase of injection duration, the influence range expands significantly but the pore pressure distribution changes little. And V_{CH_4} decreases slightly in the displaced area and the displacement velocity gradually slows down. This technique promotes multiphase flow migration in coal seam, and increases the displacement range and methane recovery efficiency.

1. Introduction

The CBM production in China is significantly lower than that in other coal-rich countries, such as Australia and the United States[1]. Due to the different geological conditions, the permeability of some coal seams is low, which determines the difficulty of methane extraction and drainage[2]. Many researchers put forward a series of enhanced coalbed methane recovery (ECBM) techniques to solve the above problems, such as large-diameter borehole drainage [3], hydraulic punching [4], pulsating shock [5], hydraulic cutting [6] (or ultra-high pressure hydraulic slitting), hydraulic fracturing [7], CO_2-ECBM[8] and pre-split blasting[9]. The basic mechanism of these techniques is to generate artificial fractures in coal seams, which can improve the permeability of coal seams and thus increase the methane recovery rate. However, methane is mainly adsorbed in nanopores of coal with high adsorption ability, which makes it difficult to effectively extract methane adsorbed[10]. Therefore, the problem of low methane recovery rate in coal seam cannot be fundamentally solved. Water displacement is considered an effective method to recover methane from small coal pores [11].

Water flooding has encountered some problems in the field practice, such as poor methane recovery rate [12]. The water diffusion in coal seam is affected by viscous force, friction force, and normal stress of fracture wall, and water lock occurs in coal seam due to capillary effect and Jiamin phenomenon [13]. Recently, some researchers use acid-base salt solutions to improve the injected water [14], which still does not completely solve the water lock damage, and only to reduce the effect of bound water [15]. CO_2 enhanced coalbed methane recovery (CO_2-ECBM) is a good alternative method to obtain a high coalbed methane recovery rate [16], involving CO_2 injected into deep coal seams [17, 18]. However, CO_2 injection can cause coal matrix expansion, which has decreased gas permeability of coal [19]. The adsorption capacity of CO_2 in coal is higher than that of

methane, which may lead to high risk of coal and gas outburst or accidental emission of CO_2 during coal mining. Considering the potential hazard of CO_2-ECBM, nitrogen injection into coal seam was proposed [14]. N_2 is mainly produced by separation from the atmosphere or decomposition of nitrogenous compounds, which requires a cost to produce, store and transport. The production of large amounts of N_2 and CO_2 is not economical. The adsorption of CH_4 and N_2 on coal matrix belongs to physical adsorption, and the adsorption capacity of CH_4 on coal matrix is stronger than that of N_2. Air containing 78% nitrogen is commonly used in field practice.

Thus, we proposed a new technique named high-pressure water and gas alternating sequestration (H-P-WGAS) in our previous work [20]. In that work, we discussed the effectiveness of the H-P-WGAS technique and verified that the H-P-WGAS technique can enhance methane migration in coal seam. The field tests indicated that the average methane drainage flow rate of single borehole increased significantly and consequently the residual methane content in coal seam decreased dramatically as a result. In the present work, the effect of injection pressure and duration on water and gas alternating sequestration of coalbed methane will be discussed, which is important to the engineering practice.

2. Numerical Model

In our study, water and air are successively injected into coal seam to displace methane. Based on the theory of multiphase-flow in porous media, the model considered fluid seepage and capillary force in coal seam, and the basic assumptions were as follow:

(1) Coal is a double porous medium rich in pores and fractures. The pore system and fracture system are assumed to be continuum systems

(2) The coal seam is homogeneous, porous, and isotropic. In-situ methane pressure and methane content are uniform everywhere in the coal seam

(3) The initial volume fraction of methane in the coal seam is 85%, and the water and air saturation are 10% and 5%, respectively

(4) Temperature of the coal seam is constant (293.15 K), and there is no heat exchange between the boundary and the coal seam

(5) Methane in the coal seam follows the ideal gas equation

2.1. Model Parameters. The coal seam model is 300 × 200 × 10 m. The plan view is shown in Figure 1. A single borehole model is established. It is a 0.1 m borehole located in the center of calculated zone (X = 150 m, Y = 100 m). Eight detection points (A to H) are arranged at different distances away from injection borehole along line L. As shown in Figure 2, the boundary pressure of coal seam is set to 2 MPa. Coal seam parameters are shown in Table 1.

2.2. Multiphase Flow Model Equation

2.2.1. Calculation Model of Fluid Seepage in Porous Media. The multiphase flow in coal seams follows Darcy's law with the continuity equation [21, 22]:

$$\frac{\partial}{\partial t}(m_l)+\nabla\bullet(\rho_l u_l) = Q_{ls} \tag{1}$$

where ρ_l is density of fluid, kg/m^3; u_l is seepage velocity of each phase, m/s, Q_{ls} is mass source of the fluid, kg/(m^3·s). m_l is liquid mass in the coal matrix per unit volume, which can be calculated by:

$$m_l = \rho_l\bullet\phi \tag{2}$$

In the present work, the swelling and deformation of the coal matrix due to water absorption are not considered, so the porosity can be expressed as:

$$\phi = \frac{(1+R_0)\phi_0 + \alpha(R-R_0)}{1+R} \tag{3}$$

where $R = \varepsilon_v + (p/K_s)$;$R_0 = \varepsilon_{v0} + (p_0/K_s)$; ε_v and ε_{v0} are volumetric strain and initial volumetric strain of coal seam, respectively; K_s is bulk modulus of coal skeleton.

The equation of permeability and porosity obtained by simultaneous formula is as follows:

$$\frac{k_l}{k_{l0}} = \left(\frac{\phi}{\phi_0}\right)^3 = \left(\frac{(1+R_0)+(\alpha(R-R_0)/\phi_0)}{1+R}\right)^3 \tag{4}$$

where k_f and k_{f_0} are the permeability and initial permeability of coal seam, respectively; ϕ and ϕ_0 are the porosity and initial porosity of coal seam, respectively.

Darcy's law for seepage in porous media is as follows:

$$q_i = -\frac{k}{\mu_i}(\nabla p + \rho_i g \nabla D) \tag{5}$$

where q_i is seepage velocity of pressure water, m/s; μ_i is hydrodynamic viscosity, Pa·s; k is permeability, mD; ρ_i is density of pressure water, kg/m^3,∇D is gravitational potential difference, m; g is gravitational acceleration, 9.8 m^2/s.

(1) and (3) can be derived as

$$\begin{aligned}\frac{\partial\phi}{\partial t} &= \frac{\alpha-\phi}{1+R}\left(\frac{\partial\varepsilon_v}{\partial t}+\frac{1}{K_s}\cdot\frac{\partial p}{\partial t}\right)\\ \rho_l\frac{\partial\phi}{\partial t} &+ \phi\frac{\partial\rho_l}{\partial t}+\nabla(\rho_l q_l) = Q_{ls}\end{aligned} \tag{6}$$

2.2.2. Multiphase Fluid Migration Model. Coal seam be regarded as a continuous porous medium with fully developed pores and fractures. The multiphase fluid seepage follows Darcy's seepage law[23]:

$$u = -\frac{\kappa_{ri}}{\mu_i}\kappa\nabla p_i \tag{7}$$

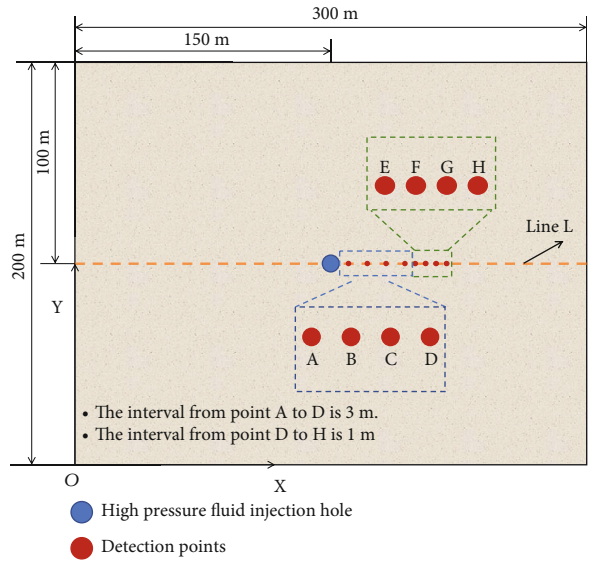

Figure 1: Detection points arrangement of the computational model. Line L: a virtual straight line along which the eight detection points (A to H) are arranged.

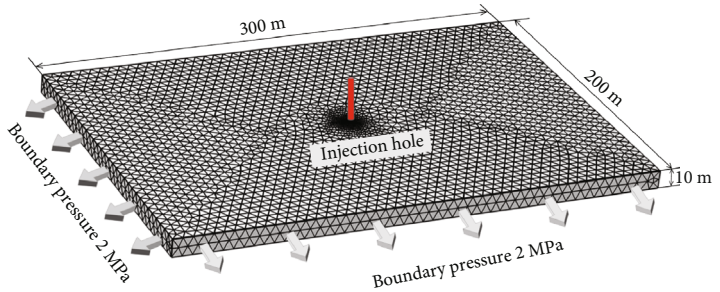

Figure 2: The 3D computational model.

where u is fluid velocity, m/s; μ_i is dynamic viscosity of the fluid, Pa·s; κ is effective permeability, mD; κ_{ri} is relative permeability, mD; ∇p_i is pressure gradient (Pa/m).

The effective permeability (κ) is related to relative permeability (κ_{ri})and can be calculated by:

$$\kappa_{ri} = \frac{\kappa_i}{\kappa} \tag{8}$$

Total methane including adsorbed methane and free methane in the coal matrix can be calculated by:

$$q = \frac{V_L q_m}{p_L + p_m} * \frac{\rho M}{V_m} + \frac{\varnothing_m M p_m}{RT} \tag{9}$$

where q is mass of methane per unit volume in coal matrix, kg/m^3; ρ is coal density, kg/m^3; V_L is Langmuir volume (maximum adsorption capacity of coal), m^3/t; p_L is Langmuir pressure, MPa; $\varnothing_m$ is porosity of the coal matrix, %; V_m is molar volume of methane under standard conditions, m^3/mol [24].

Multiphase fluid transport is based on macroscopic mass conservation equation of each phase. The average volume fraction (also known as saturation) of each phase is found.

Table 1: Coal seam parameters.

Symbol	Parameter	Value	Unit
p_c	Coal density	1250	Kg/m^3
$\varnothing$	Initial porosity	0.03	1
κ	Initial permeability	3.8e-16	m^2
ρ_m	Methane standard density	0.7	Kg/m^3
ρ_a	Air density	1.293	Kg/m^3
ρ_w	Water density	0.9814	Kg/m^3
μ_m	Methane viscosity	1.84e-5	Pa·s
μ_a	Air viscosity	1.79e-5	Pa·s
μ_w	Water viscosity	0.96e-3	Pa·s
p_{in}	Injection pressure	15	MPa
p_{out}	Boundary pressure	2	MPa
p_m	Initial seam pressure	2	MPa
t	Reference temperature	20	˚C
s_w	Initial water saturation	0.1	1
s_a	Initial air saturation	0.05	1
s_m	Initial methane volume fraction	0.85	1

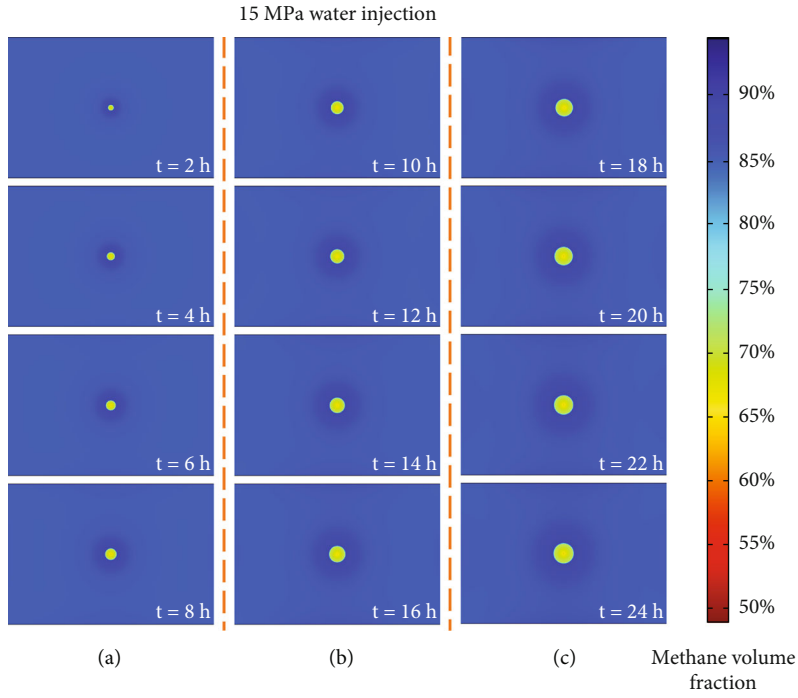

Figure 3: Contour of V_{CH_4} under water injection.

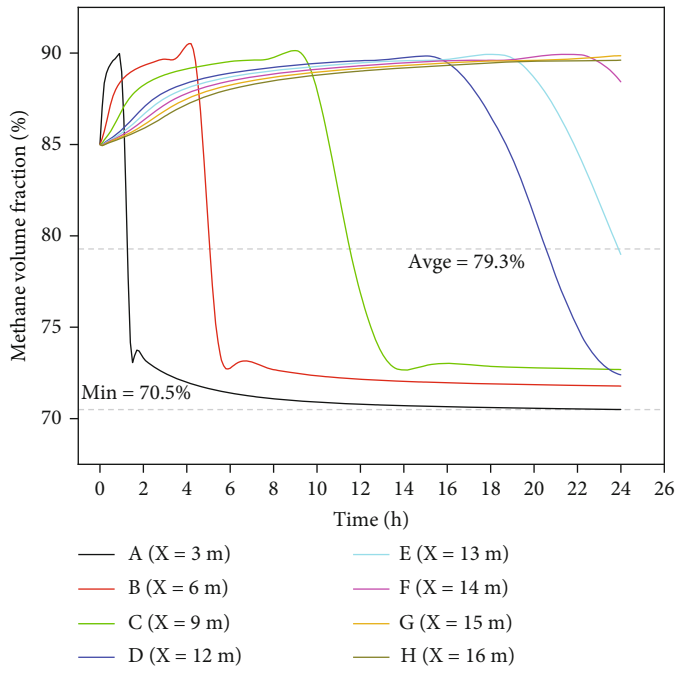

Figure 4: Time-dependent V_{CH_4} at each detection point. X =3 m: 3 m away horizontally from injection borehole. Avge: The average V_{CH_4} of all detection points at the end of the displacement (24 h).

Describe single-phase fluid transport:

$$\frac{\partial}{\partial t}(\varepsilon_i \rho_i s_i) + \nabla \bullet (\rho_i u_i) = Q_i \tag{10}$$

where ε_i (dimensionless) is porosity; ρ_i is phase density, kg/m^3; s_i is volume fraction (dimensionless); u_i represents the velocity vector of phase i, m/s; Q_i is mass source of phase i, kg/(m^3·s).

Assuming that the sum of the volume fractions of each phase is 1 (100%), the volume fraction of the remaining phase S_j is obtained by:

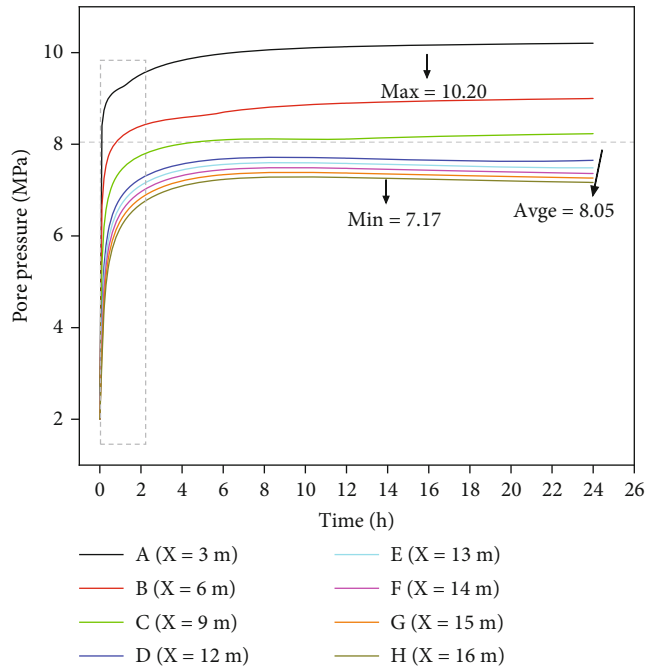

Figure 5: Time-dependent pore pressures at each detection point. Min: Minimum pore pressure in all detection points at the end of displacement.

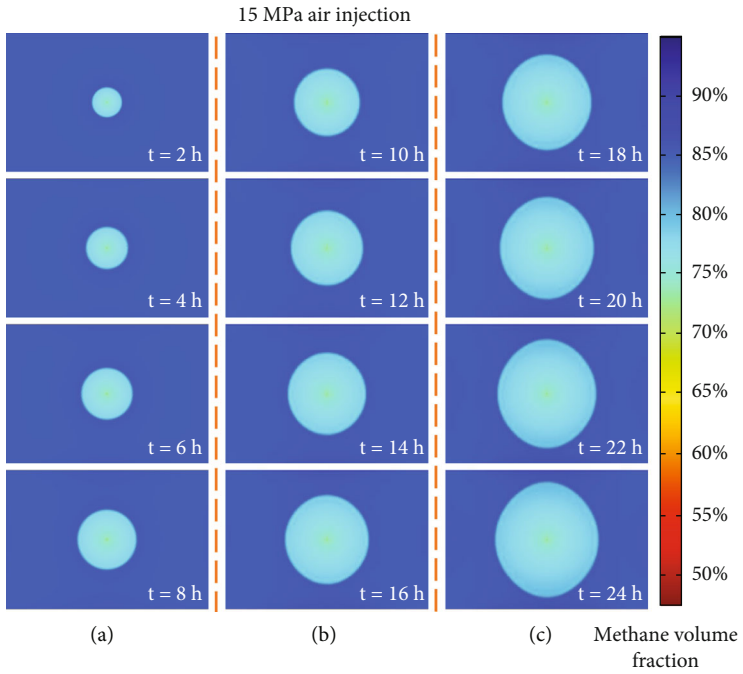

Figure 6: Contour of V_{CH_4} under air injection.

$$S_j = 1 - \left\{ \sum_{i=1.i\neq j}^{N} S_i \right\} \tag{11}$$

where S_i is volume fraction of phase i; S_j is volume fraction of phase j.

Combining (8) and (11), other N-1 phase fluid motion equations can be obtained:

$$\frac{\partial}{\partial t}(\varepsilon_i \rho_i s_i) - \nabla \cdot \left(\rho_i \kappa \frac{\kappa_{ri}}{\mu_i} \nabla p_i \right) = Q_i \tag{12}$$

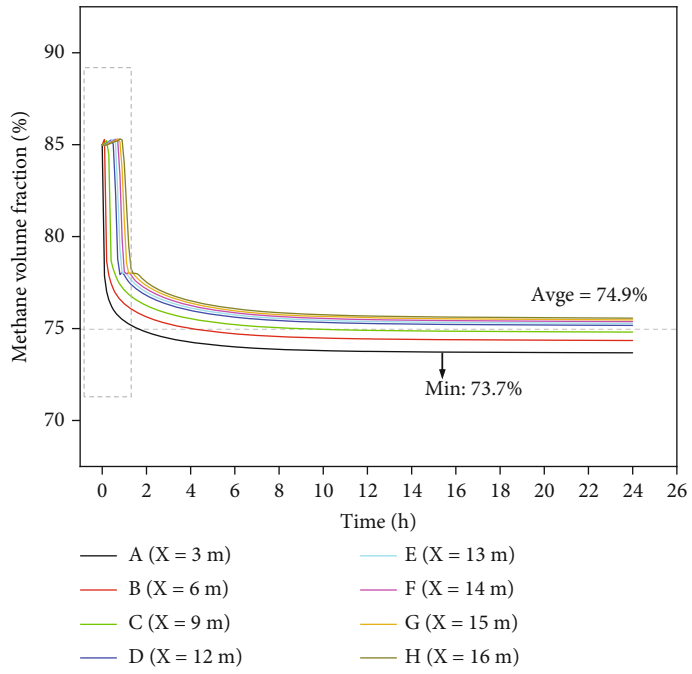

Figure 7: Time-dependent V_{CH_4} of each detection point.

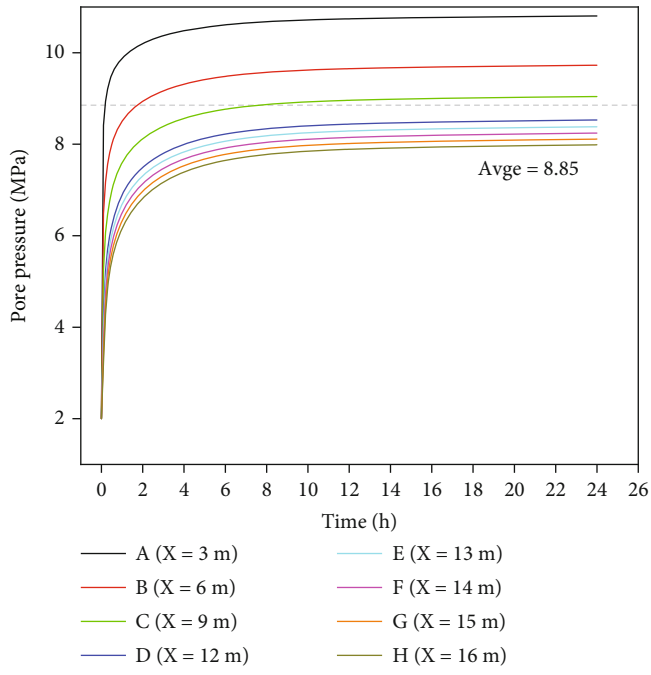

Figure 8: Time-dependent pore pressures at each detection point.

3. Results and Discussion

3.1. Comparison of Injecting Different Fluids

3.1.1. Water Injection Displacement. Figure 3 shows the evolution of methane volume fraction recorded every 2 hours. The injected water expanded from the borehole to far-field area of coal seam. The influence range of water injection expanded with the increase of injection time. As shown in Figure 4, methane fraction volume (V_{CH_4}) near the injection borehole (point A, X=3 m) decreased significantly from 85% to 73.31% after 2 hours and decreased to 70.50% after 22 hours. After 24 hours water injection, V_{CH_4} at point F to H still fluctuated around 85% and showed a slight upward trend, indicating a weak disturb by water injection. The influence effective radius of water injection is about 13 m.

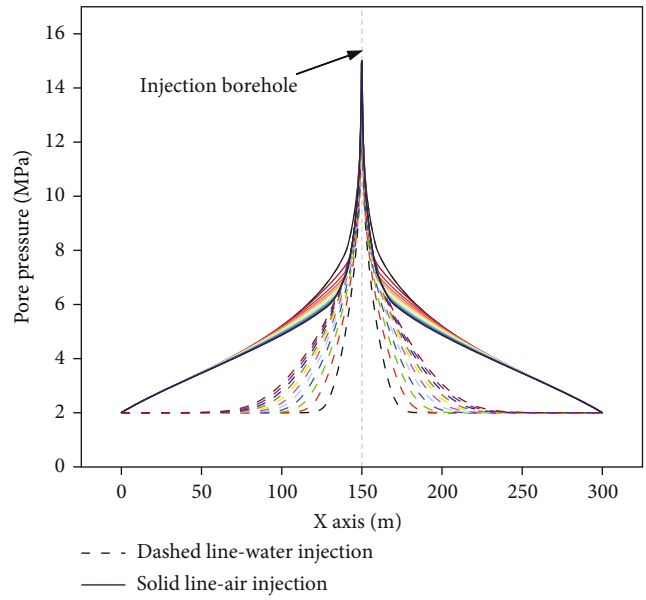

FIGURE 9: Pore pressures under water injection and air injection for 12 hours, respectively, along line L (Orange dashed line shown in Figure 1). Data is recorded and plotted every 2 hours.

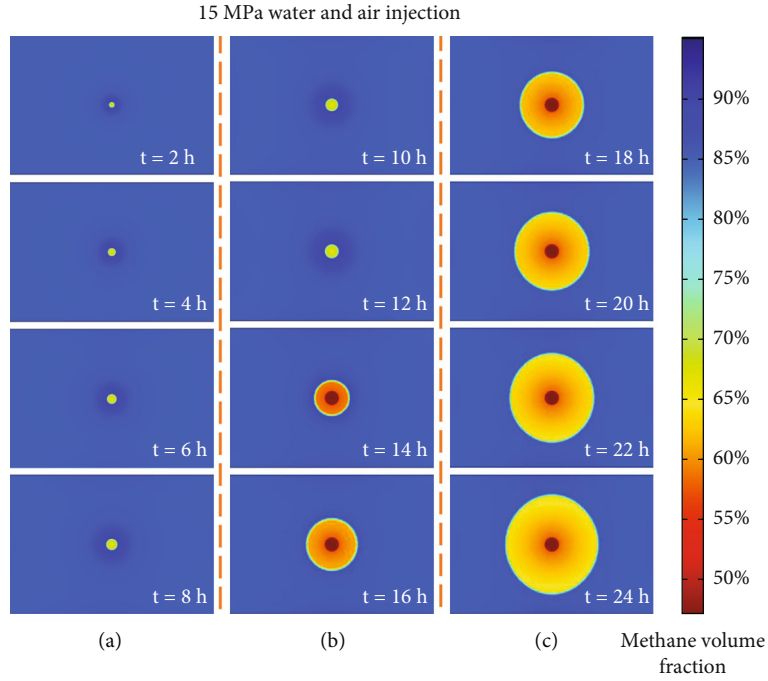

FIGURE 10: Contour of V_{CH_4} under water-air alternating displacement.

V_{CH_4} at all detection points increased at the initial stage (less than 5%) and then decreased sharply. The phenomenon also appears in the experimental studies of other scholars [11]. A reasonable explanation is: under water injection, affected by high injection pressure, pressure gradient forces the methane carried by water and the methane V_1 displaced by water to passively flow to the outside, plus the external coalbed methane V_2 that has not been affected by hydraulic permeability. Both V_1 and V_2 overlap, and the V_{CH_4} increases briefly and in a small range.

Figure 5 gives time-dependent pore pressures at different detection points. Pore pressures increased rapidly in the first two hours under high-pressure water injection, which indicates that pore pressures quickly covered all detection points

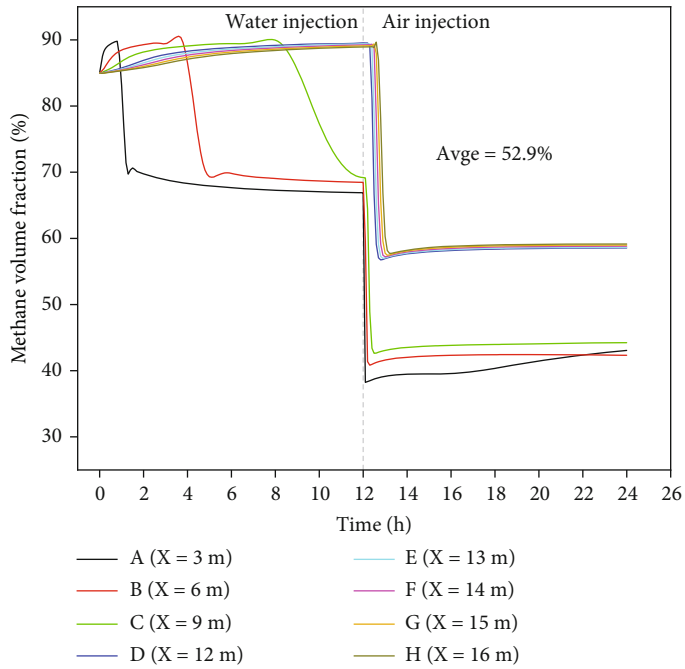

Figure 11: Time-dependent V_{CH_4} at different detection points.

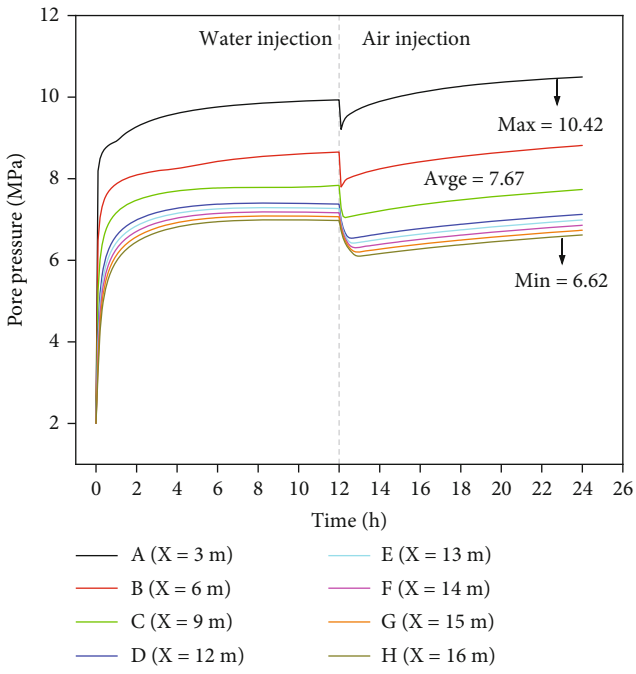

Figure 12: Time-dependent pore pressures at different detection points.

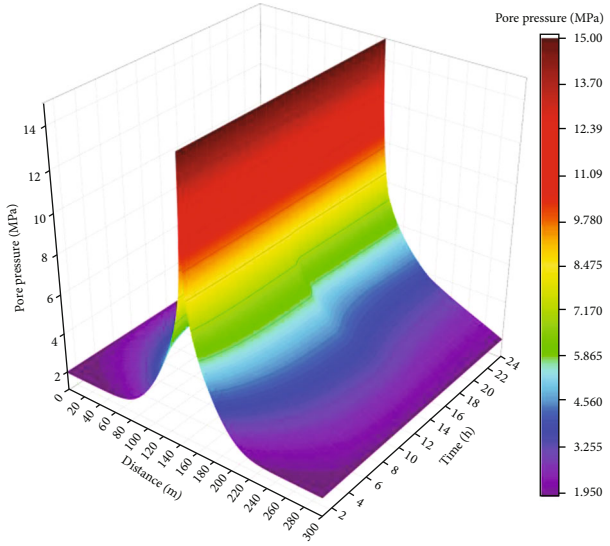

Figure 13: Time-dependent pore pressures under water-air alternating displacement.

under water injection. Pore pressure is higher in areas closer to the injection hole, which will be beneficial to fracture the coal body and extend the primary fractures.

3.1.2. Air Injection Displacement. As shown in Figure 6, the reduction of V_{CH_4} is lower than that of water displacement. The injected air expanded faster than water and had a wider displaced area. As shown in Figure 7 under air injection displacement, the decrease of V_{CH_4} fluctuated little at all detection points. V_{CH_4} decreased sharply within 2 h. The total V_{CH_4} at detection point A decreased by 90% at the first 2 h, indicating a high displacement velocity. The air expansion in coal seam is relatively uniform.

The pore pressures at different detection points finally reached a stable value when air was continuously injected.

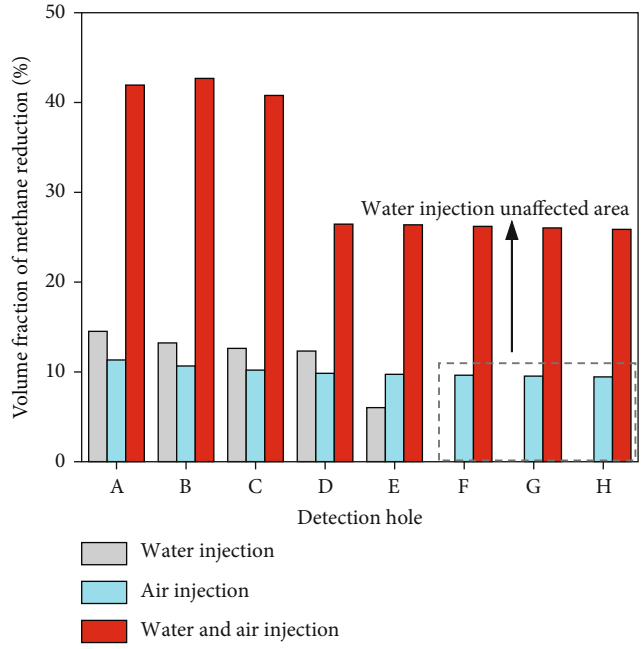

Figure 14: V_{CH_4} reduction at each detection point under three displacement methods.

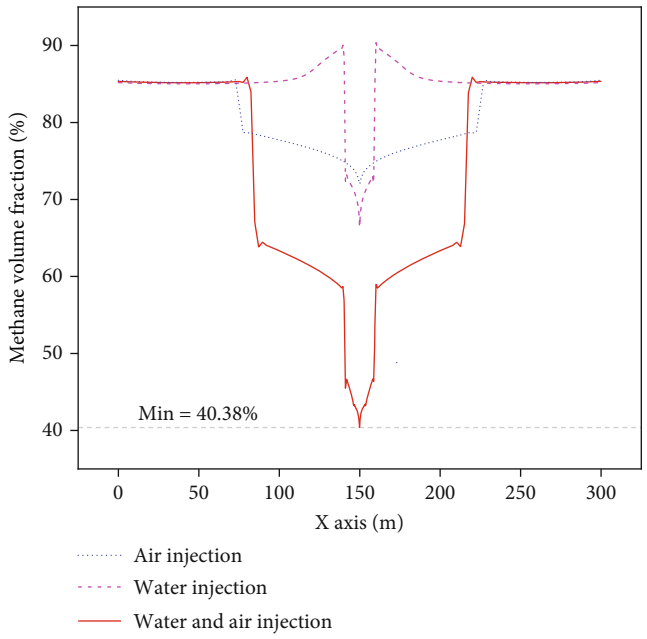

Figure 15: V_{CH_4} under three displacement methods along line L shown in Figure 1.

The average stable pore pressure of different detection points is 8.85 MPa (as shown in Figure 8), which is slightly higher than 8.05 MPa under water injection. As shown in Figure 9, the pore pressures and influence range under air injection are both significantly larger than water injection at the same injection time (12 h) along line L. The velocity of pressure propagation is obviously faster than that of water injection.

3.1.3. Characteristics of Water-Air Alternating Displacement. Water was injected into coal seam in the first 12 hours and air in the next 12 hours. As shown in Figure 10, the V_{CH_4} near the borehole decreased significantly under air injection. And the influence range was larger compared with water injection at the same time. As shown in Figure 11, V_{CH_4} at detection points A, B, and C decreased twice and stabilized at about 43%, while the average stable V_{CH_4} of other

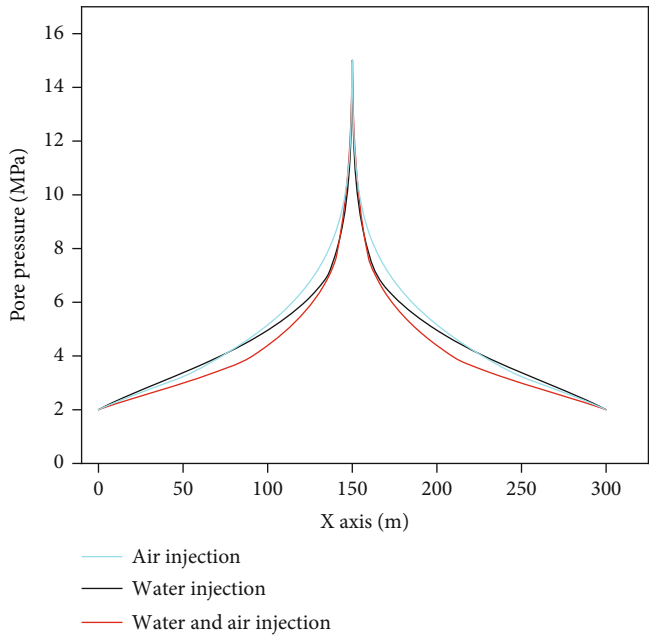

Figure 16: Pore pressures under three displacement methods at 24 h along line L.

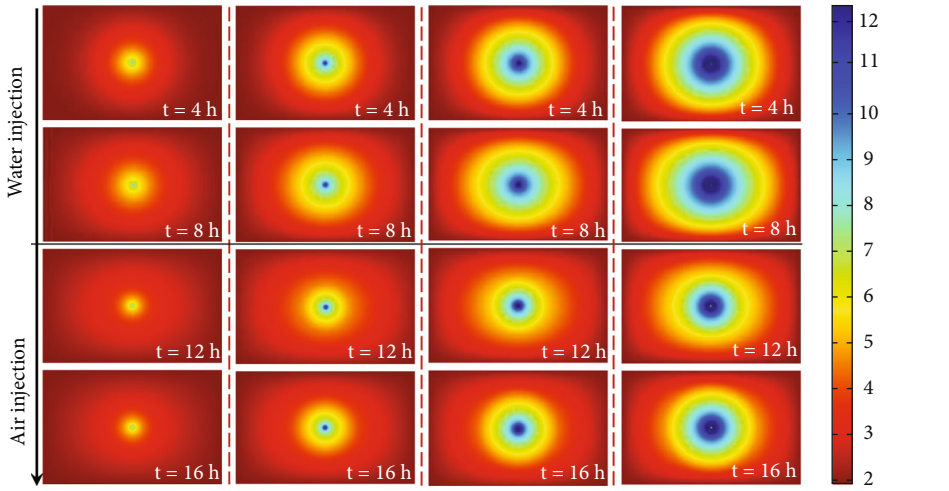

Figure 17: Contour of pore pressures under different injection pressures.

detection points was 58.5%. Under air injection (14-24 h), V_{CH_4} at different detection points did not change much, indicating that the air injection completed the displacement within two hours. This phenomenon is consistent with air injection. Therefore, WGA-ECBM technique is combined with the advantages of air injection. Under the water-air altering displacement, the average V_{CH_4} of all detection points decreased to 52.9%, while that of water injection and air injection under the same conditions decreased to 79.3% and 74.9%, respectively.

Under the water-air alternating displacement, pore pressures first increased under water injection. Pore pressures firstly decreased and then increased under air injection, as shown in Figure 12. At the time of air injection (t=12-13 h), pore pressures decreased because injected air drives the multiphase flow to migrate. According to Bernoulli equation: $p + \rho gz + (1/2) * \rho v\text{^}2 = C$, part of pressure potential energy is converted to kinetic energy. And the other part is lost when pressure gradient fractures coal body to expand the cracks and break through the water-blocked migration channel. Figure 13 shows the 3D distribution of pore pressures in coal seam. The decrease rate of pore pressure gradually slows down from borehole to the boundary.

3.1.4. Comprehensive Comparison of Three Displacement Methods. Figure 14 shows V_{CH_4} reduction at each detection

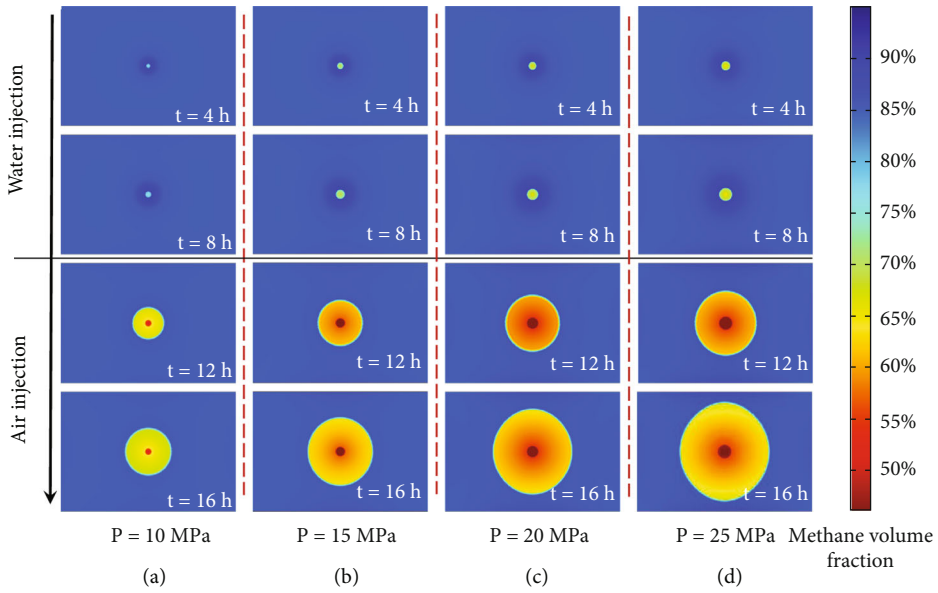

Figure 18: Contour of V_{CH_4} under different injection pressures.

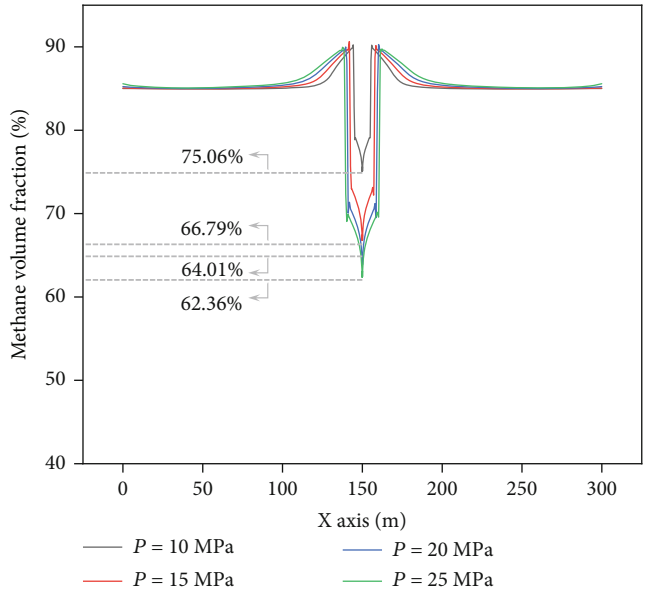

Figure 19: V_{CH_4} at the end of water injection (8 h) along line L.

point under three displacement methods. V_{CH_4} decreases most significantly under water-air alternating displacement. V_{CH_4} at detection points (F, G, H) do not decrease under water injection. However, V_{CH_4} reduction at detection points (A, B, C) is higher under water injection than under air injection.

As shown in Figure 15, V_{CH_4} in the borehole decreased to 67.16% and 72.28% under water injection and air injection, respectively. The water-air alternating displacement decreased to 40.38%. V_{CH_4} decreased again by 26.94% based on 17.84% reduction of water injection. After water injection, the aid of air injection on displacement is significant, and the second decrease in methane volume is greater. As shown in Figure 15, the influence ranges are 24.68 m, 149.73 m and 135.21 m (the diameter on L line) under water injection, air injection and water-air alternating displacement, respectively. As shown in Figure 16, pore pressure distribution under three displacement methods is similar at 24 h. This indicates that the injection pressure has completed a relatively uniform spread within 24 h.

3.2. Water-Air Alternating Displacement under Different Injection Pressures. The injection pressure affecting pore

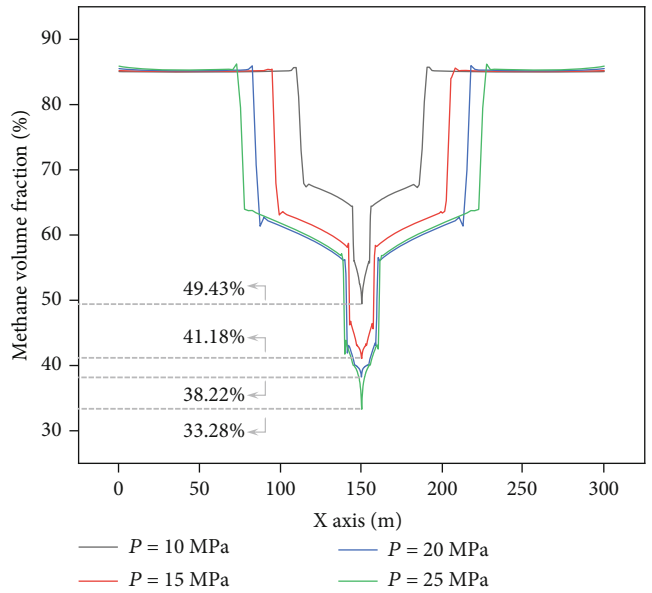

Figure 20: V_{CH_4} at the end of air injection (16 h) following water injection.

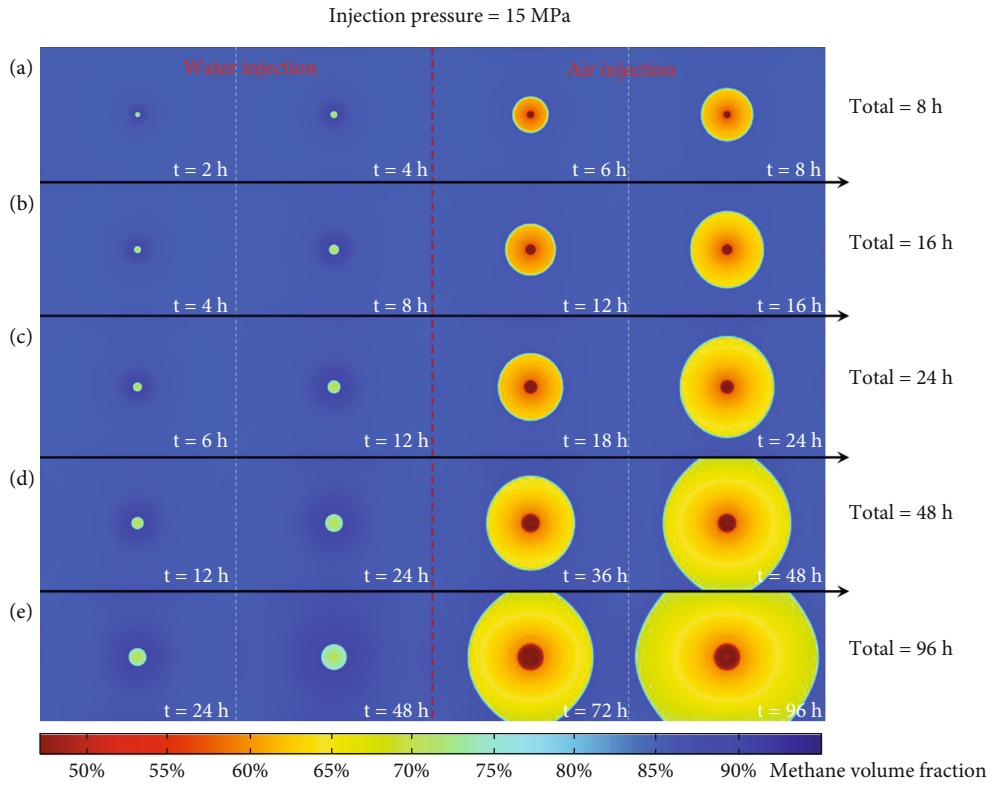

Figure 21: Contour of V_{CH_4} under different injection durations.

pressure and the permeability in coal seam is an important engineering parameter. As shown in Figure 17, the pore pressure in the contour appears to be reduced at t=12 h compared to t=8 h. The injected air pushes the methane-water in the pore space to seep outward and overcomes the capillary pressure. Resolving water-lock damage causes the pore pressures to temporarily decrease and then increase.

As shown in Figure 18, V_{CH_4} decreases gradually as injection pressure increases in a pressure gradient of 5 MPa. However, V_{CH_4} decreases slightly under water displacement. The

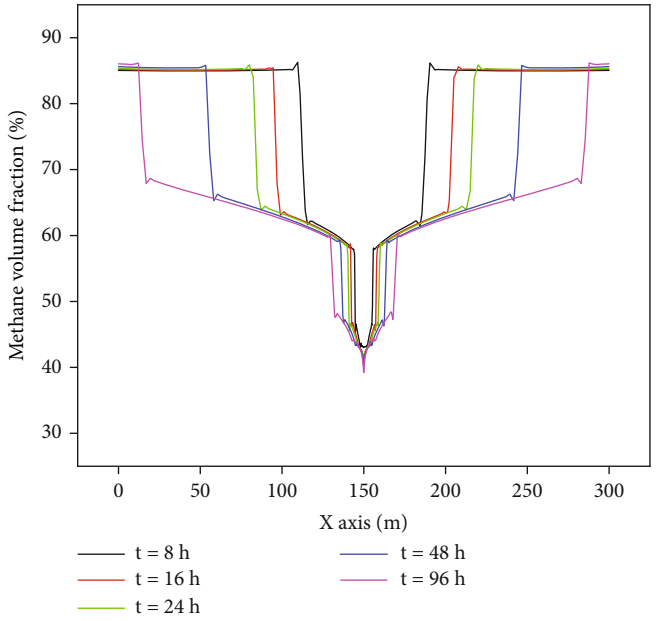

Figure 22: V_{CH_4} under water-air alternating displacement along line L.

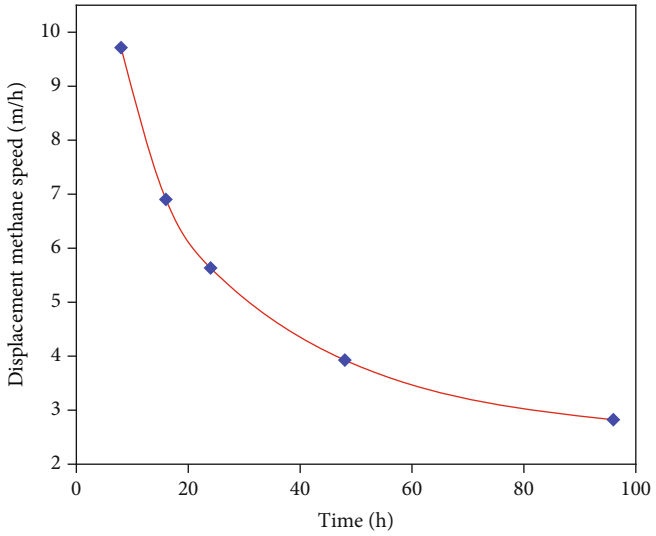

Figure 23: Average methane displacement velocity.

influence range under air injection is greater than that under water injection.

As shown in Figure 19, at the end of water injection (t = 8 h), the influence ranges from 10 MPa to 25 MPa are 10.50 m, 15.88 m, 19.82 m, and 22.27 m, respectively. V_{CH_4} in the borehole are 75.06%, 66.79%, 64.01%, and 62.36%, respectively.

As shown in Figure 20,with the foundation of the water injection, the displacement effect of the air injection is obviously better. V_{CH_4} in the borehole are 49.43%, 41.18%, 38.22% and 33.28%, respectively. The pore pressure increases as the injection pressure increases. Pressure gradient contributes to seepage (Darcy's law). The influence ranges from 10 MPa to 25 MPa are 80.92 m, 113.26 m, 135.18 m, and 154.54 m, respectively. Compared with the displacement characteristics in Figure 19, the influence range is obviously expanded.

3.3. Water-Air Alternating Displacement under Different Injection Durations. As shown in Figure 21, the influence range increases continuously with the increasing injection duration. The area expansion of the contours is significantly larger under air injection than under water injection. The air injection is more dramatically influenced by injection duration.

As shown in Figure 22, As injection duration increases in the WGA-ECBM, V_{CH_4} in the displaced area is less and less affected by the injection duration. V_{CH_4} in the borehole are

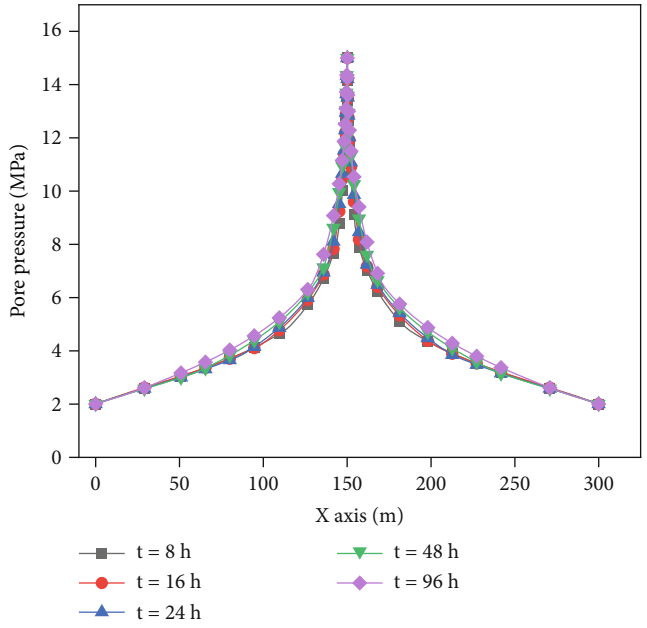

Figure 24: Pore pressures under water-air alternating displacement along line L.

42.9%, 41.2%, 40.4%, 40.3% and 39.3%, respectively. Because the adsorption and desorption of coal matrix tend to be balanced after a period of time. The injection duration ranges from 8 to 96 h, and the influence ranges are 77.72 m, 110.43 m, 135.18 m, 188.46 m and 270.90 m, respectively. However, As the wetting area of coal seam becomes larger, the seepage channels increase, and the displacement velocity gradually slows down, as shown in Figure 23. The injection duration has little effect on pore pressures. The pore pressure can propagate to the model boundary at t=8 h in Figure 24. The pore pressure distribution characteristics are similar under different injection durations.

4. Conclusions

The WGA-ECBM provide a new high-efficiency technique for the methane recovery. And in the multiphase fluid-solid coupling model, the influences of different parameters on fluid migration, pore pressure and methane content are discussed, which has important guidance value in field practice.

(1) The WGA-ECBM eliminated the high methane area generated by water injection while it also helped water injection to further expand the influence range. The influence ranges (diameter) are 24.68 m, 149.73 m and 135.21 m under water injection, air injection and water-air alternating injection, respectively. Under the same conditions, the pore pressure distribution characteristics of three methods are similar at 24 h

(2) Water-air alternating injection can quickly reduce V_{CH_4} again based on methane reduction under water injection. V_{CH_4} in the borehole are 67.16%, 72.28% and 40.38% under water injection, air injection and water-air alternating injection, respectively. The methane reduction effect of WGA-ECBM is the best among three methods

(3) The influence range of air injection is wider than water injection. The curve fluctuation of V_{CH_4} under air injection was smaller at each detection point. However, water injection is better than air injection in V_{CH_4} reduction.

(4) The influence of injection pressure and injection duration under air injection is greater than under water injection. High pressure water injection for long time is not effective. In the WGA-ECBM technique, V_{CH_4} decreases and influence range expands as the injection pressure increases in a pressure gradient of 5 MPa. With the increase of injection duration, the influence range expands significantly but the pore pressure distribution changes little. And V_{CH_4} decreases slightly in the displacement area and the displacement velocity gradually slows down

Data Availability

The data used to support the findings of this study are available from the corresponding author upon request.

Conflicts of Interest

The authors declare that they have no known competing financial interests or personal relationships that could have appeared to influence the work reported in this paper.

Acknowledgments

National Natural Science Foundation of China (NSFC) (Grant Number: 51874293, 52004176) and financial support provided by the National Science and Technology Major Project (Grant Number: 2020YFA0711803) for this research is gratefully acknowledged.

References

[1] S. Tao, S. Chen, and Z. Pan, "Current status, challenges, and policy suggestions for coalbed methane industry development in China: a review," *Energy Science & Engineering*, vol. 7, no. 4, pp. 1059–1074, 2019.

[2] Y. Li, S. Pan, S. Ning, L. Shao, Z. Jing, and Z. Wang, "Coal measure metallogeny: Metallogenic system and implication for resource and environment," *Science China Earth Sciences*, vol. 65, no. 7, pp. 1211–1228, 2022.

[3] Y. Wang, W. Yan, Z. Ren, Z. Yan, Z. Liu, and H. Zhang, "Investigation of large-diameter borehole for enhancing permeability and gas extraction in soft coal seam," *Geofluids*, vol. 2020, Article ID 6618590, 13 pages, 2020.

[4] P. Li, X. Zhang, and H. Li, "Technology of coupled permeability enhancement of hydraulic punching and deep-hole presplitting blasting in a" three-soft" coal seam," *Materials and Technology*, vol. 55, no. 1, pp. 89–96, 2021.

[5] Q. Li, X. Wu, and C. Zhai, "Effect of frequency and flow rate of pulsating hydraulic fracturing on fracture evolution," *Journal of China University of Mining & Technology*, vol. 50, pp. 1067–1076, 2021.

[6] X. Yang, Z. Yong-li, and R. Chang-zai, "The Numerical Simulation for Seepage Rule of Coal-Bed Methane with Hydraulic Cutting Seam Mining Based on Matlab," *Advanced Materials Research*, vol. 524–527, pp. 485–488, 2012.

[7] B. Hou, M. Chen, Z. Li, Y. Wang, and C. Diao, "Propagation area evaluation of hydraulic fracture networks in shale gas reservoirs," *Petroleum Exploration and Development*, vol. 41, no. 6, pp. 833–838, 2014.

[8] Y. Li, Y. Wang, J. Wang, and Z. Pan, "Variation in permeability during CO2–CH4 displacement in coal seams: part 1–experimental insights," *Fuel*, vol. 263, article 116666, 2020.

[9] C. Lian, "Study on rational technical parameters and antireflection mechanism of ultra-high pressure hydraulic slitting in high gas and soft coal seam," *China Mining Magazine*, vol. 30, pp. 144–148, 2021.

[10] Y. Li, Z. Wang, S. Tang, and D. Elsworth, "Re-evaluating adsorbed and free methane content in coal and its ad- and desorption processes analysis," *Chemical Engineering Journal*, vol. 428, article 131946, 2022.

[11] B. Huang, W. Lu, S. Chen, and X. Zhao, "Experimental investigation of the functional mechanism of methane displacement by water in the coal," *Adsorption Science & Technology*, vol. 38, no. 9-10, pp. 357–376, 2020.

[12] J. Qin and Y. Chen, "Research and application of combined antireflection technology of high pressure hydraulic fracturing and punching in low permeability coal seam," *Mining Safety & Environmental Protection*, vol. 48, no. 6, pp. 53–57, 2021.

[13] X. Su, Q. Wang, J. Song et al., "Experimental study of water blocking damage on coal," *Journal of Petroleum Science and Engineering*, vol. 156, pp. 654–661, 2017.

[14] Y. Yang, L. Si, Z. Li, J. Li, and Z. Li, "Experimental study on effect of CO2–alkaline water two-phase gas displacement and coal wetting," *Energy & Fuels*, vol. 31, no. 12, pp. 14374–14384, 2017.

[15] D. Zhao, Z. Feng, and Y. Zhao, "Experimental study of effects of high pressure water injection on desorption characteristic of coal-bed methane (CBM)," *Chinese Journal of Rock Mechanics and Engineering*, vol. 30, pp. 547–555, 2011.

[16] C. R. Clarkson and R. M. Bustin, "Binary gas adsorption/desorption isotherms: effect of moisture and coal composition upon carbon dioxide selectivity over methane," *International Journal of Coal Geology*, vol. 42, no. 4, pp. 241–271, 2000.

[17] S. Durucan and J.-Q. Shi, "Improving the CO_2 well injectivity and enhanced coalbed methane production performance in coal seams," *International Journal of Coal Geology*, vol. 77, no. 1-2, pp. 214–221, 2009.

[18] S. Zheng, Y. Yao, D. Elsworth, D. Liu, and Y. Cai, "Dynamic fluid interactions during CO2-enhanced coalbed methane and CO2Sequestration in coal seams. Part 1: CO2–CH4Interactions," *Energy & Fuels*, vol. 34, no. 7, pp. 8274–8282, 2020.

[19] Q. Niu, L. Cao, S. Sang, X. Zhou, and Z. Wang, "Anisotropic adsorption swelling and permeability characteristics with injecting CO2in coal," *Energy & Fuels.*, vol. 32, no. 2, pp. 1979–1991, 2018.

[20] C. Zhu, S. Liu, X. Chen et al., "High-pressure water and gas alternating sequestration technology for low permeability coal seams with high adsorption capacity," *Journal of Natural Gas Science and Engineering*, vol. 96, article 104262, 2021.

[21] C. Fan, L. Yang, G. Wang, Q. Huang, X. Fu, and H. Wen, "Investigation on Coal Skeleton Deformation in CO2 Injection Enhanced CH4 Drainage from Underground Coal Seam," *Frontiers in Earth Science*, vol. 9, 2021.

[22] M. Sayyafzadeh, A. Keshavarz, A. R. M. Alias, K. A. Dong, and M. Manser, "Investigation of varying-composition gas injection for coalbed methane recovery enhancement: a simulation-based study," *Journal of Natural Gas Science and Engineering*, vol. 27, pp. 1205–1212, 2015.

[23] K.-A. Lie, Ed., "Mathematical models for multiphase flow," in *An Introduction to Reservoir Simulation Using MATLAB/GNU Octave: User Guide for the MATLAB Reservoir Simulation Toolbox (MRST)*, pp. 231–271, Cambridge University Press, Cambridge, 2019.

[24] C. Hao, Y. Cheng, H. Liu, L. Wang, and Q. Liu, "A novel technology for high-efficiency borehole-enlarging to enhance gas drainage in coal seam by mechanical cutting assisted by waterjet," *Energy Sources, Part A: Recovery, Utilization, and Environmental Effects*, vol. 44, no. 1, pp. 1336–1353, 2022.